Design, Structure, and Optical Properties of Organic−Inorganic Perovskites Containing an Oligothiophene Chromophore

David B. Mitzi,* Konstantinos Chondroudis, and Cherie R. Kagan

T. J. Watson Research Center, IBM P.O. Box 218, Yorktown Heights, New York 10598

Received August 31, 1999

A quaterthiophene derivative, 5,5‴-bis(aminoethyl)-2,2′:5′,2″:5″,2‴-quaterthiophene (AEQT), has been selected for incorporation within the layered organic−inorganic perovskite structure. In addition to having an appropriate molecular shape and two tethering aminoethyl groups to bond to the inorganic framework, AEQT is also a dye and can influence the optical properties of lead(II) halide-based perovskites. Crystals of $C_{20}H_{22}S_4N_2PbBr_4$ were grown from a slowly cooled aqueous solution containing lead(II) bromide and quaterthiophene derivative (AEQT·2HBr) salts. The new layered perovskite adopts a monoclinic (*C*2/*c*) subcell with the lattice parameters $a = 39.741(2)$ Å, $b = 5.8420(3)$ Å, $c = 11.5734(6)$ Å, $\beta = 92.360(1)°$, and $Z = 4$. Broad superstructure peaks are observed in the X-ray diffraction data, indicative of a poorly ordered, doubled supercell along both the *a* and *b* axes. The quaterthiophene segment of $AEQT^{2+}$ is nearly planar, with a syn−anti−syn relationship between adjacent thiophene rings. Each quaterthiophene chromophore is ordered between nearest-neighbor lead(II) bromide sheets in a herringbone arrangement with respect to neighboring quaterthiophenes. Room temperature optical absorption spectra for thermally ablated films of the perovskites $(AEQT)PbX_4$ (X = Cl, Br, I) exhibit an exciton peak arising from the lead(II) halide sheets, along with absorption from the quaterthiophene moiety. No evidence of the inorganic sheet excitonic transition is observed in the photoluminescence spectra for any of the chromophore-containing perovskites. However, strong quaterthiophene photoluminescence is observed for X = Cl, with an emission peak at approximately $\lambda_{max} = 532$ nm. Similar photoluminescence is observed for the X = Br and I materials, but with substantial quenching, as the inorganic layer band gap decreases relative to the chromophore HOMO−LUMO gap.

Introduction

Substantial recent attention has been focused on organic−inorganic perovskites as a result of interesting and potentially useful electrical, optical, and magnetic properties that arise in these compounds.[1] The hybrid perovskites naturally form layered structures, consisting of sheets of corner-sharing metal halide octahedra separated by bilayers or monolayers of organic cations. One example, $(C_4H_9NH_3)_2(CH_3NH_3)_{n-1}Sn_nI_{3n+1}$, consists of "*n*"-layer-thick perovskite sheets interleaved with bilayers of butylammonium cations.[2] In contrast to most metal halides, which are electrically insulating, this family undergoes a semiconductor-metal transition as a function of increasing perovskite sheet thickness. The group IVA metal-based perovskites also exhibit sharp, tunable resonances in their room temperature optical absorption and emission spectra.[3] These features arise from excitonic transitions associated with the band gap of the metal halide framework and are therefore characteristic of the choice of metal and halogen making up the inorganic sheets. The strong room temperature exciton peaks in the optical spectra attest to the large exciton binding energy (>200 meV) in these self-assembling quantum well structures.

In most of the organic−inorganic systems studied to date, the relatively simple organic layer of the hybrid plays a secondary role in distinguishing the interesting physical properties associated with each compound. For example, in the known highly conducting tin(II)-based perovskites,[2] while the organic layers serve to define the dimensionality of the compound, the large conductivity arises from the small band gap and substantial carrier mobility associated with the metal halide sheets. Similarly, in the luminescent systems, the organic layers define the dimensionality of the structure and enhance the exciton binding energy through a "dielectric confinement" effect.[4] However, the strong photoluminescence arises from the radiative decay of excitons within the metal halide sheets. In each of these cases, the organic component of the structure is relatively simple, consisting of alkylammonium or single ring aromatic ammonium cations. The HOMO−LUMO energy gap for the organic molecule is therefore large compared to the band gap of the inorganic framework, and the molecules are optically and electrically inert.

One motivation of this study is to design organic dye molecules that fit within the perovskite structure and that also have the appropriate molecular energy levels so that the HOMO−LUMO gap of the organic component can be engineered relative to the band gap of the inorganic layer. The oligothiophenes are particularly useful organic moieties in this respect because the energy at which the molecules absorb (and subsequently emit) light can be controlled by choosing the length of the thiophene chain. The absorption maximum for "*n*"

* To whom correspondence should be addressed.

(1) For a recent review, see: Mitzi, D. B. *Prog. Inorg. Chem.* **1999**, *48*, 1.

(2) Mitzi, D. B.; Feild, C. A.; Harrison, W. T. A.; Guloy, A. M. *Nature* **1994**, *369*, 467.

(3) Ishihara, T. In *Optical Properties of Low-Dimensional Materials*; Ogawa, T., Kanemitsu, Y., Eds.; World Scientific: Singapore, 1995, pp 288−339.

(4) Hong, X.; Ishihara, T.; and Nurmikko, A. V. *Phys. Rev. B* **1992,** *45,* 6961.

10.1021/ic991048k CCC: $18.00
Published on Web 12/08/1999

α-linked thiophene rings varies between approximately 302 nm (4.1 eV) for $n = 2$ and 432 nm (2.9 eV) for $n = 6$.[5] This energy range is similar to that observed for the band gap and excitonic transitions in lead(II) halide perovskite sheets.[1,3] Hybrids containing oligothiophenes and lead(II) halide layers are therefore suitable for the consideration of energy and/or charge transfer between the organic and inorganic components of the structure. The issue of the resonant interaction between Wannier excitons in inorganic materials and Frenkel excitons in adjacent organic layers has recently been addressed theoretically, and it has been proposed that efficient energy transfer can be expected.[6] Charge transfer in organic−inorganic multilayers of amorphous copper phthalocyanine (CuPc) and TiO_x has also been studied and used to create a material with higher photoconductivity than the CuPc sensitizer alone.[7]

Finally, there has been substantial interest in achieving high electrical mobilities in thin films of oligothiophenes for thin film transistor (TFT) applications.[8] The degree of molecular ordering within the thin film can alter the mobility over several orders of magnitude. Many techniques have been considered for achieving well-ordered thin films of oligothiophenes. Attaching linear alkyl groups at terminal positions of the oligothiophene molecule, for example, induces the oligomers to self-organize into an arrangement with the long molecular axes roughly perpendicular to the substrate plane. This orientation leads to an increase in electrical mobility by a factor of 25 compared to the unsubstituted molecules.[9] In addition, much attention has focused on how the crystalline order depends on thin film deposition conditions, with a high degree of oligomer orientation being achieved in films deposited on heated substrates.[10] The current organic−inorganic hybrid structures provide a new opportunity to achieve robust, well-ordered, and even single crystalline layers of oligothiophene molecules, using the templating influence of the metal halide sheets. Consequently, in addition to examining the optical properties of the dye molecule within the perovskite framework, structural aspects of molecular ordering within the quaterthiophene layer will be addressed in these new materials.

Experimental Section

Synthesis.

(a) AEQT·2HX Salts. The starting AEQT·2HX salts were prepared[11] using a technique similar to that described in detail for the synthesis of 5,5‴-bis(aminomethyl)-2,2′:5′,2″:5″,2‴-quaterthiophene dihydrochloride (AMQT·2HCl).[12] The intermediate 5,5‴-bis[(2,2,5,5-tetramethyl-1-aza-2,5-disila-1-cyclopentyl)ethyl]-2,2′:5′,2″:5″,2‴-quaterthiophene was first synthesized[12,13] and then reacted in a chloroform solution with HX to form a yellow precipitate of the desired AEQT·2HX salt. The IR spectrum of each compound (in a pressed KBr pellet) is consistent with that reported for similar quaterthiophene salts.[12] IR for AEQT·2HCl: γ(CH) 791, ν(ring) 1439, $\delta(NH_3^+)$ 1599, $\nu(NH_3^+)$ 2400−3200 cm^{-1}. IR for AEQT·2HBr: γ(CH) 793, ν(ring) 1439, $\delta(NH_3^+)$ 1572, $\nu(NH_3^+)$ 2400−3200 cm^{-1}. IR for AEQT·2HI: γ(CH) 791, ν(ring) 1439, $\delta(NH_3^+)$ 1565, $\nu(NH_3^+)$ 2400−3200 cm^{-1}. The UV−vis spectrum of each compound in water also yields an absorption peak similar to that previously observed[12] in AMQT·2HCl and AEQT·2HCl: AEQT·2HCl, 395 nm; AEQT·2HBr, 396 nm; AEQT·2HI, 396 nm.

(b) (AEQT)$PbBr_4$ Crystals. (AEQT)$PbBr_4$ crystals were grown from a slowly cooled, saturated, aqueous solution containing the organic and inorganic salts. First, 14.5 mg (0.025 mmol) of AEQT·2HBr and 18.3 mg (0.050 mmol) of $PbBr_2$ were weighed and added to a test tube under an inert atmosphere. The contents were dissolved in the sealed tube at 120 °C in a solvent mixture of 22 mL of deionized water, 1 mL of ethylene glycol, and 2 drops of 48% aqueous HBr, forming a nominally saturated yellow solution. Upon slow cooling at 2 °C/h to 0 °C, small, yellow, sheetlike crystals of the desired (AEQT)$PbBr_4$ compound formed. To prevent deforming the thin crystals, the product was removed from the reaction tube using a pipet and deposited on filter paper. After the paper absorbed the solution, (AEQT)$PbBr_4$ crystals remained behind and could be examined and selected for X-ray diffraction under an optical microscope.

(c) Thin Film Deposition. Films of AEQT·2HX and (AEQT)PbX_4 (X = Cl, Br, and I) were prepared for optical measurement using the single source thermal ablation (SSTA) technique, which has recently been demonstrated as an effective process for depositing a wide variety of organic−inorganic hybrids.[14,15] Quartz substrates were cleaned by sonication in 2% (w/v) detergent solution in water (20 min), followed by sonication in acetone (20 min) and ethanol (20 min). They were subsequently boiled in ethanol (5 min) and placed in a 130 °C oven to dry. Suspensions of the AEQT·2HX (X = Cl, Br, I) and (AEQT)PbX_4 (X = Cl, Br, I) compounds were made by adding 0.003 g of the materials to 0.1 mL of methanol, followed by sonication for 10 min. The charge was placed dropwise via a syringe on the tantalum heater of the SSTA chamber. The chamber was then closed and evacuated with a rotary mechanical pump until all the solvent evaporated (typically about 2 min). A turbomolecular pump was then switched on, and the system was pumped to approximately 10^{-7} Torr. To initiate the evaporation, a large current of approximately 65 A was passed through the heater for about 4 s. The deposited AEQT·2HX films were thermally annealed at 150 °C for 5 min on a digitally controlled hot plate in a nitrogen-filled glovebox. The (AEQT)PbX_4 films were annealed at 150 (5 min), 180 (15 min), and 200 °C (30 min) for X = Cl, Br, and I, respectively. These temperatures correspond to the minimum temperature/time values needed to observe the exciton feature (characteristic of the perovskite structure) in the UV−vis absorption spectrum. Film thickness, measured with a Tencor P-10 stylus profilometer, varied between 500 and 900 Å. IR spectra of the thermally ablated films (on NaCl disks) were identical to those of the starting materials examined in a KBr pellet, indicating that the organic cation remains intact after the ablation process.

X-ray Crystallography. An (AEQT)$PbBr_4$ crystal, with the approximate dimensions 0.01 mm × 0.27 mm × 0.30 mm, was selected under a microscope and attached to the end of a quartz fiber with 5 min epoxy. A full sphere of data was collected at room temperature on a Bruker SMART CCD diffractometer, equipped with a normal focus 2.4 kW sealed tube X-ray source (Mo Kα radiation). The crystal was maintained in a gentle stream of ambient temperature dry nitrogen gas during the measurement. Intensity data were collected with a detector distance of approximately 5.0 cm, in 2384 frames with increasing ω, and an exposure time of 120 s per frame. The increment in ω between each frame was 0.3°. Instrument and crystal stability were monitored, and the maximum variations in I were <0.5%.

Examination of the CCD frames indicates the existence of two types of reflections. One set consists of sharp, strong, well-defined peaks arising from a subcell with the lattice parameters $a = 39.741(2)$ Å, $b = 5.8420(3)$ Å, $c = 11.5734(6)$ Å, and $\beta = 92.360(1)°$. The second set of spots corresponds to a superstructure, which doubles the cell along both the a and b axes, yielding the refined cell parameters $a =$

(5) Grebner, D.; Helbig, M.; Rentsch, S. *J. Phys. Chem.* **1995**, *99*, 16991.
(6) (a) Agranovich, V. M.; Basko, D. M.; La Rocca, G. C.; Bassani, F. *J. Phys.: Condens. Matter* **1998**, *10*, 9369. (b) Agranovich, V. M.; La Rocca, G. C.; Bassani, F. *JETP Lett.* **1997**, *66*, 749.
(7) Takada, J.; Awaji, H.; Koshioka, M.; Nakajima, A.; Nevin, W. A. *Appl. Phys. Lett.* **1992**, *61*, 2184.
(8) Garnier, F. *Chem. Phys.* **1998**, *227*, 253.
(9) Garnier, F.; Yassar, A.; Hajlaoui, R.; Horowitz, G.; Deloffre, F.; Servet, B.; Ries, S.; Alnot, P. *J. Am. Chem. Soc.* **1993**, *115*, 8716.
(10) Servet, B.; Horowitz, G.; Ries, S.; Lagorsse, O.; Alnot, P.; Yassar, A.; Deloffre, F.; Srivastava, P.; Hajlaoui, R.; Lang, P.; Garnier, F. *Chem. Mater.* **1994**, *6*, 1809.
(11) Liang, K.; Mitzi, D. B. Unpublished work.
(12) (a) Muguruma, H.; Saito, T.; Sasaki, S.; Hotta, S.; Karube, I. *J. Heterocycl. Chem.* **1996**, *33*, 173. (b) Muguruma, H.; Saito, T.; Hiratsuka, A.; Karube, I.; Hotta, S. *Langmuir* **1996**, *12*, 5451.
(13) Muguruma, H.; Kobiro, K.; Hotta, S. *Chem. Mater.* **1998**, *10*, 1459.
(14) Mitzi, D. B.; Prikas, M. T.; Chondroudis, K. *Chem. Mater.* **1999**, *11*, 542.
(15) Chondroudis, K.; Mitzi, D. B. *Chem. Mater.*, in press.

Table 1. Crystallographic Data for the (AEQT)$PbBr_4$ Subcell

chem formula	$C_{20}H_{22}S_4N_2PbBr_4$	Z	4
fw	945.5	ρ_{calcd}, g/cm^3	2.339
space group	*C2/c* (No. 15)	wavelength (Å)	0.710 73 (Mo Kα)
a, Å	39.741(2)	absorp coeff (μ), cm^{-1}	125.9
b, Å	5.8420(3)	R_f[a]	0.044
c, Å	11.5734(6)	R_w[b]	0.063
β, deg	92.360(1)	goodness of fit (GoF)[c]	2.80
V, Å^3	2684.7(2)		

[a] $R_f = \Sigma(F_o - F_c)/\Sigma(F_o)$. [b] $R_w = \{\Sigma w(F_o - F_c)^2/\Sigma(wF_o^2)\}^{1/2}$. [c] GoF $= \{\Sigma w(F_o - F_c)^2/(n - m)\}^{1/2}$, where n = number of reflections and m = number of refinement parameters.

79.502(4) Å, b = 11.6868(6) Å, c = 11.5752(6) Å, and β = 92.340(1)°. While a number of these superstructure peaks are strong, the reflections exhibit broad or substantially split ω scans, suggesting a poorly ordered superstructure. Several (AEQT)PbX_4 crystals for both X = Br and I were examined, and each exhibited a similar distinction between subcell and supercell reflections. Note that the CCD detector is ideally suited for detecting systems with partially ordered superstructures, since the superstructure peaks become streaklike in certain frames, while the subcell peaks remain sharp. While the X = Br structure has been refined using both the subcell and supercell parameters, the subcell results are presented here because the refinement stability and final parameters (*R*-factors, goodness of fit, etc.) are superior. The final subcell parameters and crystal orientation matrix were obtained by a least-squares fit of 8192 reflections. An empirical absorption correction, based on equivalent reflections, was applied to the intensity data.[16]

The structure was solved and refined using the NRCVAX 386 PC version program.[17] First, the Pb and Br atoms were located using direct methods. The N and C atoms were then located using a single Fourier difference map. All non-hydrogen atoms were refined anisotropically. Hydrogen atoms for the quaterthiophene unit and the ammonium group at the end of the AEQT molecule were identified using Fourier difference maps, while the hydrogens for the disordered ethyl fragment were placed at idealized positions. During refinement, the positional and thermal parameters of the quaterthiophene hydrogens were fully refined, whereas those of the other hydrogens (associated with the disordered ethylammonium fragment) were not refined. The minimum and maximum peaks in the final difference Fourier map corresponded to −3.67 and +2.26 e/Å^3, with the first five residual peaks all appearing within 1.0 Å of either Pb or Br(1). No additional symmetry was detected using the MISSYM program.[18] The crystallographic results are summarized in Table 1. The atomic coordinates, heavy atom anisotropic displacement parameters, and important bond distances and angles are listed in Tables 2−4, respectively.

Optical Properties. Absorption spectra were obtained at room temperature on the thermally ablated films of AEQT·2HX and (AEQT)PbX_4 (X = Cl, Br, and I), using a Hewlett-Packard UV−vis 8543 spectrophotometer. Photoluminescence (PL) and excitation (PLE) spectra were recorded at room temperature on a Spex Fluorolog-2 spectrofluorometer using the front-face geometry. Light from a xenon arc lamp was used as the excitation source, after being passed through a SPEX 1680 0.22 m double monochromator. The emission was passed through a similar monochromator and detected with a SPEX 1911F photomultiplier tube (PMT).

Low-temperature fluorescence measurements were also performed on microcrystalline samples of the hybrid perovskite (AEQT)$PbBr_4$. A thin deposit of the crystals was formed on a sapphire window by pressing and smearing crystals of the perovskite between two windows. The deposit on sapphire was then mounted on a coldfinger and cooled with an APD Cryogenics displex system to approximately 30 K.

Table 2. Positional and Thermal Parameters[a] for (AEQT)$PbBr_4$

atom	x	y	z	B_{iso}(Å^2)
Pb	0.50	0.48689(5)	0.25	4.01(2)
Br(1)	0.42349(2)	0.4882(1)	0.24827(7)	4.20(3)
Br(2)	0.50001(3)	0.6209(2)	0.00077(8)	3.17(5)
Br(3)	0.49961(4)	0.9846(2)	0.1908(1)	3.29(5)
S(1)	0.34543(5)	0.9865(2)	0.3261(2)	3.55(6)
S(2)	0.29034(4)	0.8832(3)	0.1156(1)	3.40(6)
N(1a)	0.4368(2)	0.817(2)	0.4863(8)	3.2(4)
N(1b)	0.4367(3)	0.984(2)	0.416(1)	3.4(5)
C(1a)	0.4229(6)	1.056(3)	0.479(2)	4.2(8)
C(1b)	0.4227(5)	1.020(3)	0.532(2)	3.8(7)
C(2a)	0.3893(7)	1.081(3)	0.524(2)	2.2(6)
C(2b)	0.383(1)	1.087(7)	0.518(4)	6.9(16)
C(3)	0.3634(2)	0.920(1)	0.4596(6)	3.3(2)
C(4)	0.3521(2)	0.714(1)	0.4952(6)	3.9(3)
C(5)	0.3297(2)	0.606(1)	0.4171(6)	3.9(3)
C(6)	0.3230(2)	0.732(1)	0.3195(5)	3.1(2)
C(7)	0.2994(2)	0.683(1)	0.2227(5)	3.0(2)
C(8)	0.2797(2)	0.492(1)	0.2065(7)	3.5(3)
C(9)	0.2573(2)	0.5079(9)	0.1097(7)	3.3(2)
C(10)	0.2594(1)	0.709(1)	0.0511(5)	3.0(2)

[a] All atoms are refined anisotropically. Selected anisotropic thermal parameters are listed in Table 3. A full list of anisotropic thermal parameters can be found in Supporting Information Table S.3.

Table 3. Selected Anisotropic Displacement Parameters, U_{ij} (×100),[a] for (AEQT)$PbBr_4$

atom	U_{11}	U_{22}	U_{33}	U_{12}	U_{13}	U_{23}
Pb(1)	10.33(4)	2.42(2)	2.49(2)	0.00(0)	0.38(2)	0.00(0)
Br(1)	4.38(4)	7.09(5)	4.49(4)	−0.63(3)	−0.02(3)	−0.42(3)
Br(2)	4.91(7)	4.59(7)	2.56(6)	−0.48(5)	0.07(5)	−0.08(4)
Br(3)	5.03(8)	2.45(5)	5.06(7)	0.07(4)	0.81(6)	−0.03(4)
S(1)	4.54(9)	4.23(9)	4.70(10)	−0.92(6)	−0.17(7)	−0.11(6)
S(2)	4.33(9)	3.65(8)	4.94(9)	−1.15(6)	0.03(7)	−0.06(6)

[a] The anisotropic displacement factor expression is as follows: $\exp[-2\pi^2(U_{11}h^2(a^*)^2 + U_{22}k^2(b^*)^2 + U_{33}l^2(c^*)^2 + 2U_{12}hk\,a^*b^* + 2U_{13}hla^*c^* + 2U_{23}klb^*c^*)]$.

Results and Discussion

Synthetic Issues. A number of structural factors constrain the design of organic cations for incorporation within the layered perovskite framework.[1] First, the molecule must contain one or two unobstructed ammonium units (or other cationic hydrogen bonding components) so that reasonably strong hydrogen bonding can occur between these groups and the perovskite sheet halogens. The ammonium groups must fit into the spaces provided by the terminal and bridging halogens, without the rest of the molecule sterically hindering the formation of the inorganic sheets. For example, $(C_6H_5C_2H_4NH_3)_2CuBr_4$ adopts the layered perovskite structure,[19] since the phenethylammonium cation effectively bonds to the inorganic layer without the phenyl ring interfering with the terminal bromides. In contrast, $(C_6H_5C_2H_4NH_2CH_3)_2CuBr_4$ assumes a structure[20] with isolated $CuBr_4^{2-}$ anions, since the added methyl group impedes hydrogen bonding between the ammonium group and the halogens of a hypothetical perovskite layer. One of the easiest ways to ensure unimpeded hydrogen bonding is to attach the ammonium group using a sufficiently long alkylammonium chain—that is either as $R-(CH_2)_nNH_3^+$ or as $^+NH_3(CH_2)_n-R-(CH_2)_nNH_3^+$. For monoammonium cations, the organic cations hydrogen bond to only one inorganic layer, leading to a bilayer of organic cations between the perovskite sheets and a van der Waals gap between the layers. For the diammonium cations, the organic cations span the entire distance between and bond to two adjacent inorganic sheets.

(16) Sheldrick, G. M. "*SADABS*"; Institut für Anorganische Chemie der Universität Göttingen: Göttingen, Germany, 1997.
(17) Gabe, E. J.; Le Page, Y.; Charland, J.-P.; Lee, F. L.; White, P. S. *J. Appl. Crystallogr.* **1989**, *22*, 384.
(18) Le Page, Y. *J. Appl. Crystallogr.* **1988**, *21*, 983.
(19) Willett, R. D. *Acta Crystallogr.* **1990**, *C46*, 565.
(20) Place, H.; Willett, R. D. *Acta Crystallogr.* **1988**, *C44*, 34.

Table 4. Selected Bond Distances (Å) and Angles (deg) for (AEQT)$PbBr_4$[a]

Pb(1)−Br(1)	3.0397(8)	C(3)−C(4)	1.36(1)
Pb(1)−Br(1)[a]	3.0397(8)	C(4)−C(5)	1.39(1)
Pb(1)−Br(2)	2.989(1)	C(5)−C(6)	1.364(9)
Pb(1)−Br(2)[c]	2.970(1)	C(6)−C(7)	1.459(8)
Pb(1)−Br(3)[a]	2.987(1)	C(7)−C(8)	1.374(9)
Pb(1)−Br(3)[d]	3.014(1)	C(8)−C(9)	1.40(1)
N(1a)−C(1a)	1.50(2)	C(9)−C(10)	1.362(9)
N(1b)−C(1b)	1.49(3)	C(10)−C(10)[h]	1.45(1)
C(1a)−C(2a)	1.46(4)	S(1)−C(3)	1.719(7)
C(1b)−C(2b)	1.61(5)	S(1)−C(6)	1.733(6)
C(2a)−C(3)	1.56(2)	S(2)−C(7)	1.732(6)
C(2b)−C(3)	1.41(4)	S(2)−C(10)	1.741(6)

Br(1)−Pb(1)−Br(1)[a]	179.70(2)	C(1a)−C(2a)−C(3)	112(1)
Br(1)−Pb(1)−Br(2)	91.88(3)	C(1b)−C(2b)−C(3)	114(3)
Br(1)[a]−Pb(1)−Br(2)[c]	91.96(3)	S(1)−C(3)−C(2a)	122(1)
Br(1)[a]−Pb(1)−Br(3)[a]	90.01(3)	S(1)−C(3)−C(2b)	119(2)
Br(1)−Pb(1)−Br(3)[d]	90.30(3)	S(1)−C(3)−C(4)	110.1(5)
Br(1)[a]−Pb(1)−Br(2)	88.04(3)	C(2a)−C(3)−C(4)	128(1)
Br(1)−Pb(1)−Br(2)[c]	88.10(3)	C(2b)−C(3)−C(4)	131(2)
Br(1)−Pb(1)−Br(3)[a]	89.70(3)	C(3)−C(4)−C(5)	114.5(6)
Br(1)[a]−Pb(1)−Br(3)[d]	89.99(3)	C(4)−C(5)−C(6)	113.1(6)
Br(2)−Pb(1)−Br(2)[c]	177.06(4)	S(1)−C(6)−C(5)	110.1(5)
Br(2)−Pb(1)−Br(3)[d]	92.05(4)	S(1)−C(6)−C(7)	121.0(4)
Br(2)[c]−Pb(1)−Br(3)[a]	88.99(4)	C(5)−C(6)−C(7)	128.8(6)
Br(2)[c]−Pb(1)−Br(3)[d]	90.89(4)	S(2)−C(7)−C(6)	121.7(4)
Br(2)−Pb(1)−Br(3)[a]	88.07(4)	S(2)−C(7)−C(8)	110.5(5)
Br(3)[d]−Pb(1)−Br(3)[a]	179.88(4)	C(6)−C(7)−C(8)	127.6(6)
Pb(1)−Br(2)−Pb(1)[b]	152.57(5)	C(7)−C(8)−C(9)	113.1(6)
Pb(1)[g]−Br(3)[a]−Pb(1)	153.60(6)	C(8)−C(9)−C(10)	114.0(5)
C(3)−S(1)−C(6)	92.2(3)	S(2)−C(10)−C(9)	110.3(5)
C(7)−S(2)−C(10)	92.1(3)	S(2)−C(10)−C(10)[h]	119.2(4)
N(1a)−C(1a)−C(2a)	115(2)	C(9)−C(10)−C(10)[h]	130.5(6)
N(1b)−C(1b)−C(2b)	110(2)		

[a] Symmetry transformations: (a) $1-x, y, 0.5-z$; (b) $1-x, 1-y, -z$; (c) $x, 1-y, 0.5+z$; (d) $x, -1+y, z$; (g) $x, 1+y, z$; (h) $0.5-x, 1.5-y, -z$.

In addition to the requirement of an appropriate tethering group for hydrogen bonding to the inorganic layers, the organic R group must also have an appropriate shape to fit within the perovskite structure. The projection of the organic molecule on a plane along one molecular axis (or the "cross-sectional area" of the molecule) should be smaller than the nominally square area defined by the terminal halogens from four adjacent corner-sharing MX_6 octahedra. One edge of the square is approximately twice the average bridging interatomic M−X distance. If the cross-sectional area of the organic molecule is much smaller than this square, the structure can accommodate by allowing the organic molecules to tilt or interdigitate, thereby more effectively filling the available space. On the other hand, if the area required by the organic molecule is too large, the perovskite structure may not be able to adapt (i.e. neighboring molecules will sterically interfere) and a different structural type is likely to result. Therefore, for the layered perovskite framework, organic molecules with a long and narrow profile are preferable to those that are wide and bulky.

Chemical interactions between the R groups of the organic cations can also influence the overall structure in the solid state and ultimately either stabilize or destabilize the perovskite framework. The polymerized $(HOOCCH{=}CHCH{=}CHCH_2NH_3)_2CdCl_4$ perovskite structure, for example, is stabilized by hydrogen bonding between COOH groups on adjacent organic sheets.[21] Other types of interactions that can influence the overall organic−inorganic structure include van der Waals and aromatic−aromatic interactions between the R groups.

In accordance with these structural constraints, oligothiophene molecules represent an appropriate class of potential R groups. With one or two alkylammonium tethering units attached to the oligothiophene molecule, the resulting organic cation is expected to fit within a layered perovskite framework. In this study, an oligothiophene molecule with two alkylammonium groups (one on each end) has been examined because of the relative stability of α,ω-substituted oligothiophenes, as well as the relative ease with which symmetrically substituted thiophene compounds can be synthesized. Ultimately, a short ethylammonium tethering group was adopted to facilitate electronic interaction between the organic and inorganic components of the structure, without compromising the stability of the perovskite framework.

Finally, when considering the possibility of energy/charge transfer, the energy levels of the organic cation relative to the inorganic framework need to be considered. The lead(II) halide-based layered perovskites (with optically inert organic cations) exhibit a strong exciton peak in their absorption spectra at approximately 332 (X = Cl), 405 (X = Br), and 504 nm (X = I).[1] The absorption (and subsequent emission) from oligothiophene molecules can be tailored according to the number of thiophene units in the molecule (e.g. 302 nm for $n = 2$ to 432 nm for $n = 6$).[5] For quaterthiophene (in solution), the peak absorption is at approximately 390 nm. This molecule is an interesting choice for the lead(II) halide-based perovskite structures since, for X = Cl, the inorganic layer exciton peak falls at a higher energy than the quaterthiophene absorption peak, for X = Br, the electronic transitions are approximately equal, and, for X = I, the exciton peak is at a lower energy than the quaterthiophene transition. Combining the structural and energetic considerations for the organic dye molecule, we selected the 5,5‴-bis(aminoethyl)-2,2′:5′,2″:5″,2‴-quaterthiophene (AEQT) molecule for incorporation within the organic−inorganic perovskite framework.

Crystal Structure. Single-crystal structure analysis for (AEQT)$PbBr_4$ establishes that the AEQT cation fits as envisioned within the layered perovskite structure (Figure 1). The inorganic framework consists of the characteristic $PbBr_4^{2-}$ perovskite sheets. Each lead(II) atom is surrounded by a slightly distorted octahedral coordination of bromides (see Table 4), with bond lengths ranging from 2.970(1) to 3.040(1) Å [3.006(1) Å average]. Both bridging bromides in the subcell model, Br(2) and Br(3), are refined as disordered over two symmetry-related sites ("a" and "b"), with an occupancy fixed at 0.5. In contrast, both the lead(II) atom and the terminal bromide, Br(1), are not disordered. Note that while the thermal parameters are generally well-behaved, the lead(II) atom has a slightly elongated profile along the *a* axis (Table 3). Presumably, this elongation, as well as the apparent disordering of the bridging bromide ions, results because the actual structure has a poorly developed superstructure that is not accounted for in the current model.

Notice that the bridging Pb−Br−Pb bond angles are substantially different from 180° [i.e. 152.57(5) and 153.60(6)°], indicating that adjacent octahedra are substantially rotated relative to each other. As for the recently described $(C_6H_5C_2H_4NH_3)_2PbCl_4$ structure,[22] the ethylammonium tail for each organic cation sits nominally in a distorted square defined by four nearest-neighbor lead(II) atoms and the Pb−Br−Pb linkages between them (Figure 2). The square can be either "pinched-

(21) (a) Tieke, B.; Chapuis, G. *Mol. Cryst. Liq. Cryst*. **1986**, *137*, 101. (b) Tieke, B.; Chapuis, G. *J. Polym. Sci., Polym. Chem. Ed.* **1984**, *22*, 2895.

(22) D. B. Mitzi, *J. Solid State Chem.* **1999**, *145*, 694.

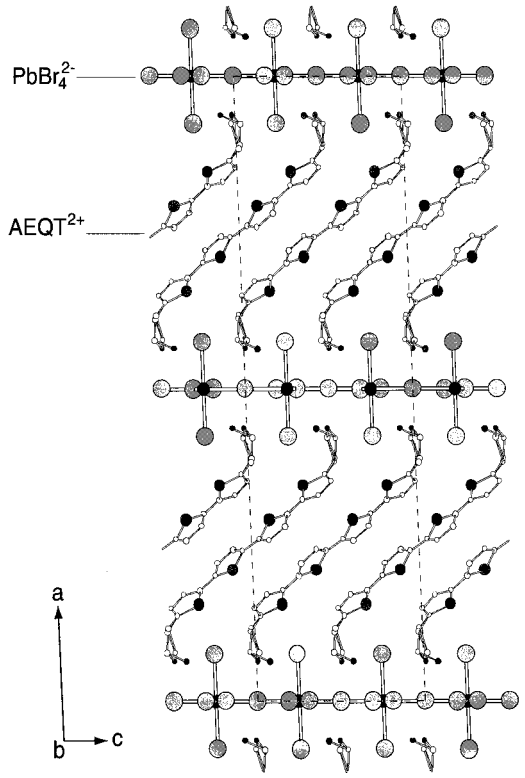

Figure 1. Crystal structure of (AEQT)$PbBr_4$ viewed down the *b* axis. The unit cell outline is shown by the dashed lines. For clarity, the atoms are represented as spheres with uniform sizes selected for each atom type.

in" along the *c* axis and "pushed-out" along the *b* axis (Figure 2a) or "pushed-out" along the *c* axis and "pinched-in" along the *b* axis (Figure 2b). A mixture of these two possibilities within a given square is unlikely [i.e. a square defined by either Pb, Br(2a), Br(3b) or Pb, Br(2b), Br(3a)] since this would lead to a short [3.058(2) or 3.198(2) Å] Br···Br contact (note that $2R_{Br}$ = 3.92 Å, where R_{Br} is the ionic radius for a Br^- ion[23]) . In addition, this configuration would result in an unreasonable geometry for hydrogen bonding to the organic cation (see below).

The bridging bromides must therefore be distributed (with equal probability) between the two geometries described in Figure 2. Within a given sheet, the distortion of one square (defined by one set of four $PbBr_6$ octahedra) fixes the distortion for each nearest-neighbor square of octahedra (i.e. they must be in the opposite configuration). Consequently, each sheet should be ordered and the apparent bromide disorder (or lack of a well-defined superstructure) can most reasonably be attributed to a loss of registry between adjacent perovskite sheets rather than from disorder within a given sheet. This loss of registry is not surprising since the organic cation is long and has a tethering group on each end that can take several different conformations.

In fact, the relatively rigid quaterthiophene component of the AEQT molecule is fully ordered within the subcell model, while the ethylammonium tethering group is disordered over two different conformations. These two conformations correspond to the two possible geometries for the lead(II) bromide framework (Figure 2). In both ethylammonium conformations, the C(2) carbons (nearest to the quaterthiophene unit) are nominally in the plane of the quaterthiophene molecule, while

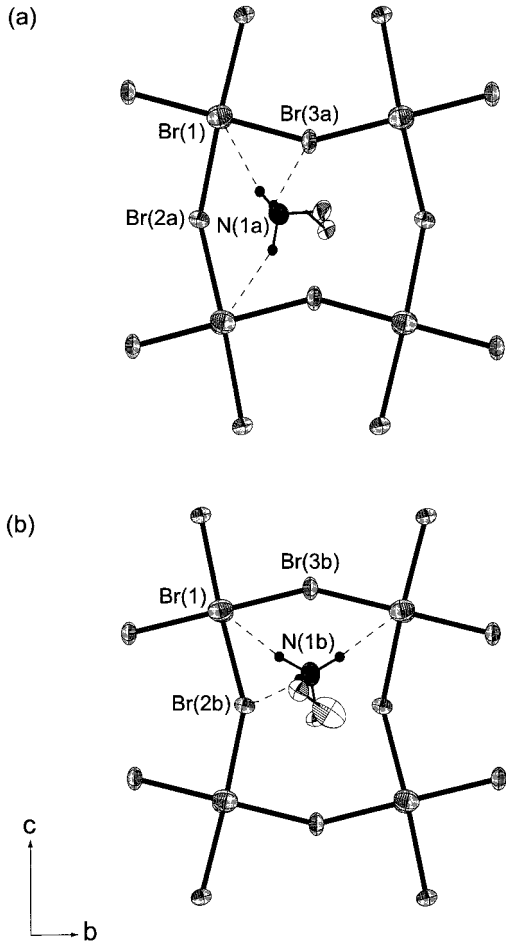

Figure 2. Two configurations for the lead(II) bromide framework and the $AEQT^{2+}$ ethylammonium tail (a,b). The primary hydrogen bonding interactions between the ammonium head of each AEQT cation and the bromines in the perovskite sheet are shown as dashed lines. The unrefined positions of the hydrogen atoms have been determined from the final Fourier difference map, and these atoms are drawn as spheres with arbitrary size. For clarity, only the ethylammonium fragment of each AEQT cation and the ammonium group hydrogens are shown. The thermal ellipsoids for the non-hydrogen atoms are drawn at 50% probability.

the rest of the alkylammonium tail is directed out of this plane. One of the two equally populated ethylammonium terminations results in hydrogen bonding to two terminal Br(1) and one bridging Br(3a) bromine (Figure 2a). In this case, the plane containing the three ammonium hydrogens is nominally parallel to the *c* axis. The second termination results in hydrogen bonding to two terminal Br(1) and one bridging Br(2b) bromine (Figure 2b), resulting in the plane containing the ammonium hydrogens being nominally parallel to the *b* axis. In both cases, the hydrogen bonding provides an example of a "terminal halogen" hydrogen bonding configuration (hydrogen bonding to two terminal and one bridging halogen) rather than a "bridging halogen" configuration (hydrogen bonding to two bridging and one terminal halogen).[1] This can be associated with the rather bulky nature of the organic cation and the rigid nature of the inorganic framework. For N(1a), the N···Br distances to the closest three bromides are 3.38(1) [Br(1)], 3.46(1) [Br(3a)], and 3.58(1) Å [Br(1)]. Similar N···Br distances occur for N(1b).

The structural picture that emerges, then, is one in which an ordered sheet of lead(II) bromide octahedra templates the conformation of the ethylammonium fragment attached to each AEQT molecule. The other end of the long molecule is nominally independent and in principle can nucleate the

(23) Shannon, R. D. *Acta Crystallogr.* **1976**, *A32*, 751.

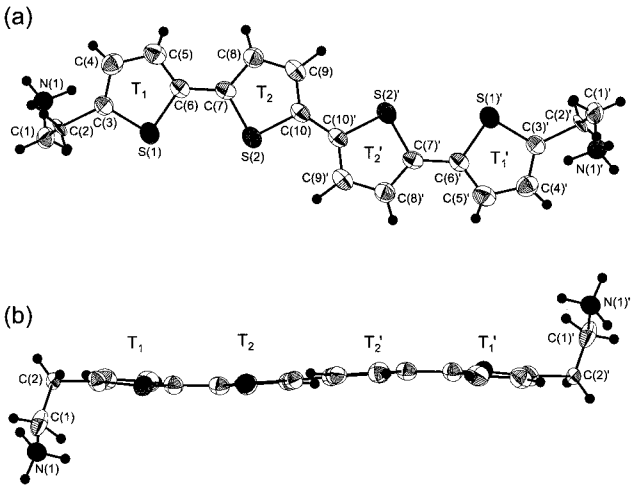

Figure 3. Top (a) and side (b) view of the doubly protonated 5,5‴-bis(aminoethyl)-2,2′:5′,2″:5″,2‴-quaterthiophene molecule in (AEQT)-$PbBr_4$. The thermal ellipsoids for the non-hydrogen atoms are drawn at 50% probability, while the hydrogen atoms are drawn as spheres with arbitrary size. Only one of the two orientations of the $AEQT^{2+}$ ethylammonium tail is shown.

formation of an inorganic sheet that is either in phase or out of phase with the layer beneath it (relative to the checkerboard arrangement of the two inorganic fragments shown in Figure 2). The degree to which adjacent layers are in registry establishes how well the superstructure peaks can establish themselves. Whereas the $(C_6H_5C_2H_4NH_3)_2PbCl_4$ unit cell exhibits a $2a_p \times 2a_p$ superstructure in the plane of the perovskite sheet, as a result of the fully ordered alternating arrangement of the "pinched-in" and "pushed-out" squares both within and between inorganic sheets,[22] in the (AEQT)$PbBr_4$ subcell structure, there is only a $2a_p \times a_p$ ordering. The fact that the supercell peaks (corresponding to a $2a_p \times 2a_p$ in-plane structure) are much broader suggests that the registry between layers is not perfect.

Oligothiophene Conformation and Ordering. The conformation of the protonated 5,5‴-bis(aminoethyl)-2,2′:5′,2″:5″,2‴-quaterthiophene molecule in (AEQT)$PbBr_4$ is shown in Figure 3. Each quaterthiophene oligomer can be fully described by two independent thiophene rings T_1\{S(1), C(3), C(4), C(5), C(6)\} and T_2\{S(2), C(7), C(8), C(9), C(10)\}. The other half of the quaterthiophene oligomer is generated by symmetry from the *C*2/*c* space group, yielding the rings T_1'\{S(1)′, C(3)′, C(4)′, C(5)′, C(6)′\} and T_2'\{S(2)′, C(7)′, C(8)′, C(9)′, C(10)′\}. The backbone conformation among the four rings is syn−anti−syn. Each thiophene ring is essentially planar, with all non-hydrogen atoms falling within 0.01(1) Å of the least−squares best plane. The dihedral angle between the planes defined by the two thiophene rings, T_1 and T_2 (or T_1' and T_2'), is 9.0(2)°. This angle is accomplished by a combination of a tilting of the connecting C(6)−C(7) [C(6)′−C(7)′] bond, out of the plane of the central two thiophene rings (T_2 and T_2'), as well as by a rotation about this bond axis.

In general, there are several factors involved in determining the conformation of the oligothiophene molecules. The first is the influence of π-electron conjugation between the rings, which tends to favor an entirely planar conformation. The second influence involves the steric hindrance between hydrogen and sulfur atoms on adjacent rings. In addition, in the solid state, there is the potential for interaction between adjacent quaterthiophene molecules and the influence of the hydrogen bonding interactions through the attached ethylammonium groups. These latter processes are expected to favor a distortion from planarity. The slight deviation from a planar geometry in the current

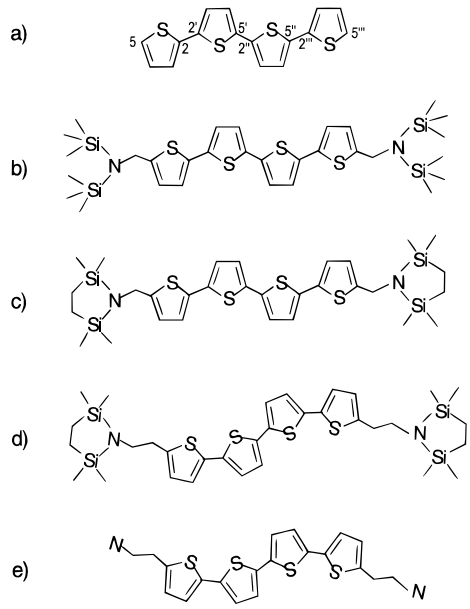

Figure 4. Molecular representation of (a) α-quaterthiophene, (b) 5,5‴-bis[*N*,*N*-bis(trimethylsilyl)aminomethyl]-2,2′:5′,2″:5″,2‴-quaterthiophene, (c) 5,5‴-bis[(2,2,5,5-tetramethyl-1-aza-2,5-disila-1-cyclopentyl)-methyl]-2,2′:5′,2″:5″,2‴-quaterthiophene, (d) 5,5‴-bis[(2,2,5,5-tetramethyl-1-aza-2,5-disila-1-cyclopentyl)ethyl]-2,2′:5′,2″:5″,2‴-quaterthiophene, and (e) 5,5‴-bis(aminoethyl)-2,2′:5′,2″:5″,2‴-quaterthiophene within the (AEQT) $PbBr_4$ structure. In (a), the numbering scheme of the quaterthiophene molecule is shown.

structure can be considered a compromise between these competing factors.

The syn−anti−syn geometry is somewhat uncommon among the oligothiophenes. Generally, as a result of steric interactions, the all-anti (or all-trans) geometry can be regarded as the lowest energy configuration—i.e., for a strictly coplanar pair of thiophene rings, the syn configuration is characterized by one short H···H contact and an interaction between sulfur lone pairs, whereas for the anti configuration these interactions are replaced by two (lone pair)···H interactions.[24] In the solid state, the all-anti conformation is adopted for α-quaterthiophene (Figure 4a).[25] The compounds 5,5‴-bis[(2,2,5,5-tetramethyl-1-aza-2,5-disila-1-cyclopentyl)methyl]-2,2′:5′,2″:5″,2‴-quaterthiophene and 5,5‴-bis[*N*,*N*-bis(trimethylsilyl)aminomethyl]-2,2′:5′,2″:5″,2‴-quaterthiophene (Figure 4b,c), which have bulky terminal groups attached to the quaterthiophene, also exhibit similar all-anti conformations.[13] However, 5,5‴-bis[(2,2,5,5-tetramethyl-1-aza-2,5-disila-1-cyclopentyl)ethyl]-2,2′:5′,2″:5″,2‴-quaterthiophene (Figure 4d) has recently been shown[13] to adopt a nearly planar (dihedral angle of 5.0° between least-squares best planes containing adjacent thiophene rings) syn−anti−syn conformer, similar to that observed in (AEQT)$PbBr_4$. It is interesting to note that both of these syn−anti−syn quaterthiophene compounds have two terminal ethyl groups, each attached to a nitrogen atom. A "noncoplanar" syn−anti−syn conformation has also been observed for a β-methyl-substituted quaterthiophene, with a dihedral angle of 54.2° between mean planes through adjacent rings.[26] In addition, 3′4″-didecyl-2,2′:5′,2″:5″,2‴-quaterthiophene has recently been found to consist of mixture of all-anti and syn−anti−syn conformers.[27]

(24) Barone, V.; Lelj, F.; Russo, N.; Toscano, M. *J. Chem. Soc., Perkin Trans. 2* **1986**, 907.
(25) Siegrist, T.; Kloc, C.; Laudise, R. A.; Katz, H. E.; Haddon, R. C. *Adv. Mater.* **1998,** *10,* 379.
(26) Barbarella, G.; Zambianchi, M.; Bongini, A.; Antolini, L. *Adv. Mater.* **1993**, *5*, 834.

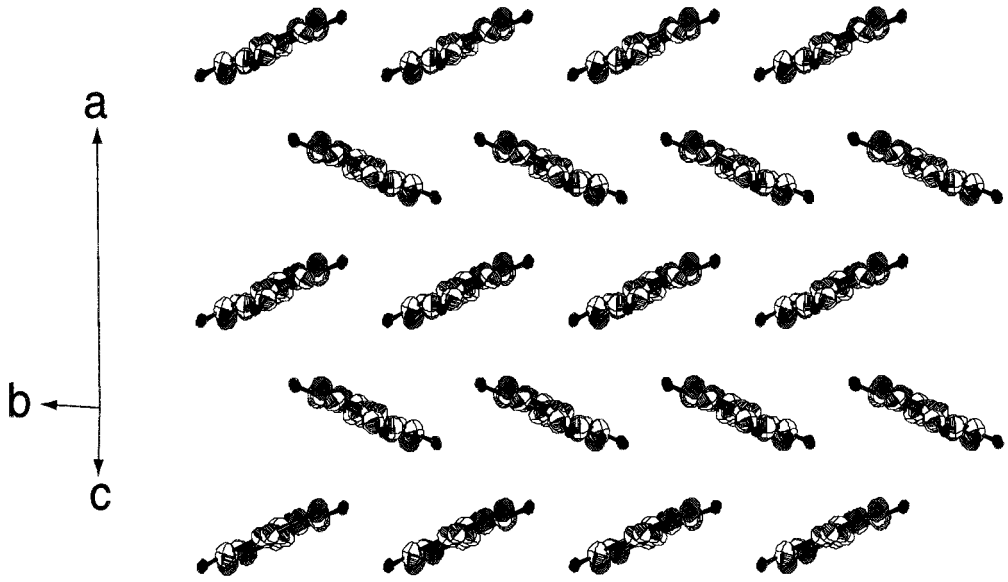

Figure 5. View down the long molecular axis of one layer of AEQT cations in the $(AEQT)PbBr_4$ structure. For clarity, only the quaterthiophene component of the AEQT molecule is drawn, clearly demonstrating the herringbone arrangement of the quaterthiophene units in the structure.

Within each thiophene ring, the S−C distances (Table 4) range from 1.719(7) to 1.741(6) Å, consistent with other oligothiophenes.[13,25−28] The thiophene C═C bond lengths are all similar [1.36(1)−1.37(1) Å], as are the thiophene intraring C−C bonds [1.39(1)−1.40(1) Å] and the interring C−C bonds [1.45(1)−1.46(1) Å]. For the anti-related thiophene rings, T_2 and T_2', the S(2)···S(2)′ distance is 4.377(3) Å. However, for adjacent syn-related rings, T_1 and T_2 (T_1' and T_2'), there is a short S(1)···S(2) interaction distance [3.263(2) Å], which is substantially shorter than twice the van der Waals radius for sulfur (∼1.8 Å).[29] Presumably, this steric interaction is one factor leading to the tilting and rotation of adjacent syn-related thiophene rings, relative to a perfectly planar conformation. Note that a very similar short S···S interaction can also be inferred from the published positional parameters for the syn−anti−syn quaterthiophene derivative, 5,5‴-bis[(2,2,5,5-tetramethyl-1-aza-2,5-disila-1-cyclopentyl)ethyl]-2,2′:5′,2″:5″,2‴-quaterthiophene.[13]

The quaterthiophene oligomers pack into the layered organic−inorganic framework such that the oligomers are substantially tilted relative to the perovskite sheet normal. The least-squares plane through the quaterthiophene section of the AEQT molecule (averaging over the slight misorientation of the planes defined by the T_1 and T_2 rings) provides a dihedral angle of 44.53(6)° with respect to the plane containing the Pb, Br(2), and Br(3) atoms (i.e. the plane of the perovskite sheets). Viewing down the length of the quaterthiophene molecules, the oligomers in $(AEQT)PbBr_4$ adopt a herringbone arrangement (Figure 5), similar to that observed in purely organic crystals and films of the various oligothiophenes.[28,30−32] The closest contacts between quaterthiophene oligomers include C(7)···C(9)[d] [3.580(9) Å] and S(2)···C(8)[d] [3.586(8) Å]. These values are close to the sum of the van der Waals radii for each atom (∼1.7 Å for carbon and ∼1.8 Å for sulfur[29]). The closest intermolecular S···S interaction is S(1)···S(2)[a] [4.148(3) Å].

A crystal of the analogous lead(II) iodide compound, $(AEQT)PbI_4$, has also been grown and examined using single-crystal X-ray diffraction. The iodide crystal exhibits an isostructural monoclinic (*C*2/*c*) subcell to that of the bromide, with the dimensions, $a = 38.814(3)$ Å, $b = 6.0946(5)$ Å, $c = 12.331(1)$ Å, and $\beta = 92.318(2)°$. Broad supercell reflections, which double the *a* and *b* axes, are also noted. As might be expected, the *b* and *c* axes (in the plane of the perovskite sheets) increase with the substitution of the larger iodide ion for the bromide ion. The *a* axis, however, decreases by approximately 1 Å in going from the bromide to the iodide. Clearly, this must be related to a change in conformation or orientation of the AEQT molecule within the structure. In fact, the conformation of the molecule is very similar for the two compounds, with the iodide compound exhibiting a dihedral angle of 9.4(5)° between the best least-squares planes for the nearly planar inner (T_2) and outer (T_1) thiophene rings. The dihedral angle between the perovskite sheet and the least-squares best plane containing the quaterthiophene moiety, however, is substantially smaller in the iodide [40.15(9)°] compared to the bromide [44.53(6)°]. Taking the length of the quaterthiophene derivative as approximately the distance between the C(2) and C(2)′ atoms for a given quaterthiophene molecule [16.5 Å] and the quaterthiophene tilt angle as the angle between the line connecting these two atoms and the plane of the perovskite sheet, then the difference in separation between adjacent perovskite sheets as the tilt angle is reduced from 42.0 (X = Br) to 37.7° (X = I) is approximately 1 Å. Since there are two organic layers per unit cell, the total reduction in the *a* axis dimension arising within the organic layers is ∼2 Å. At the same time, there is an increase in the *a* axis as a result of the four larger Pb−X(1) bond lengths per unit cell [3.2551(8) Å for Pb−I(1) versus 3.0397(8) Å for Pb−Br(1)]. The combination of these two competing shifts leads to the overall ∼1 Å reduction of the unit cell dimension along the *a* axis when iodide replaces bromide in the organic−inorganic structure.

Optical Properties. The optical spectra of the lead(II) halide-based perovskites with optically inert organic molecules are dominated by an excitonic transition associated with the band

(27) Wang, S.; Brisse, F.; Bélanger-Gariépy, F.; Donat-Bouillud, A.; Leclerc, M. *Acta Crystallogr.* **1998**, *C54*, 553.
(28) Antolini, L.; Horowitz, G.; Kouki, F.; Garnier, F. *Adv. Mater.* **1998**, *10*, 382.
(29) Bondi, A. *J. Phys. Chem.* **1964**, *68*, 441.
(30) Barclay, T. M.; Cordes, A. W.; MacKinnon, C. D.; Oakley, R. T.; Reed, R. W. *Chem. Mater.* **1997**, *9*, 981.
(31) Hotta, S.; Waragai, K. *Adv. Mater.* **1993**, *5*, 896.
(32) Porzio, W.; Destri, S.; Mascherpa, M.; Brückner, S. *Acta Polym.* **1993**, *44*, 266.

gap of the inorganic framework. These excitons are rather mobile and have a two-dimensional Bohr radius (~10−20 Å)[3,4] which extends over several metal(II) halide octahedra in the plane of the perovskite sheet, suggesting that they are nominally Wannier-like in character. The exciton binding energies are large for these materials [e.g. $E_b = 320$ meV for $(C_nH_{2n+1}NH_3)_2PbI_4$], enabling the radiative decay of the excitons (i.e. peaks in the absorption and photoluminescence spectra) to be observed at room temperature. The exciton peak in the absorption spectrum for $(C_4H_9NH_3)_2PbX_4$ shifts from 504 nm (X = I), to 405 nm (X = Br) and 332 nm (X = Cl).[1] The exciton peak can also be shifted by varying other parameters of the extended inorganic framework (e.g. making substitutions for the lead(II) atom or changing the thickness of the perovskite sheet). Consequently, the exciton peak can be tuned quasi-continuously over much of the visible and near-UV region.[33] A corresponding peak is generally observed in the room temperature photoluminescence spectrum with a small Stokes shift compared to the absorption spectrum.

In contrast, the luminescence from organic dye molecules generally originates from $\pi^* \rightarrow \pi$ electronic transitions within the molecule and consequently can be considered to result from nominally localized (or Frenkel) exciton states. For a given organic molecule, changes in the optical properties of the molecule in different systems generally arise from changes in the conformation of the molecule or changes in the local environment. The oligothiophene derivative 3,3′,4″,3‴-tetrakis-(methylsulfanyl)-2,2′:5′,2″:5″,2‴-quaterthiophene, for example, exists in two different crystalline forms, depending on the solvent used for crystal growth.[34] In the triclinic form, the inner thiophene rings are exactly coplanar, whereas the terminal ones are twisted by 28.9°. In the monoclinic form, the quaterthiophene backbone is more distorted, with the external rings twisted by 57° with respect to the inner ones. Due to the more substantial loss of π-conjugation in the monoclinic form, the optical features associated with the HOMO−LUMO gap are blue shifted by about 140 nm in this compound compared to the triclinic form.

The room temperature absorption spectra (Figure 6a−c) for thermally ablated films of the current quaterthiophene dye salts AEQT·2HX (X = Cl, Br, I) are virtually identical, with a series of peaks at approximately 365 (strong), 420 (shoulder), and 459 nm (weak). These absorption spectra are distinct from the spectra of the dye salts in solution (Figure 6d), which nominally consist of a single peak centered at 395 nm. The strong absorption band in the solution spectrum is attributed to the $\pi-\pi^*$ transition of the quaterthiophene chromophore. The splitting of this band into a weak lower energy band and a stronger higher energy band, in the solid state, has also been observed in crystalline thin films of α-quaterthiophene (α-4T) and can be associated with dye aggregation and/or electron−phonon interactions.[35,36]

A corresponding splitting of the optical spectrum is observed in the photoluminescence excitation spectra for the dye salt thin films (Figure 7). The positions of the excitation spectral features are in good agreement with those of the absorption spectra. The room temperature emission spectra of the thin films also exhibit three broad peaks: 487 (weak), 538 (strong), and 576 nm (medium). The spectra for each of the three salts (only X = Cl is shown) are virtually identical. The relatively weak high-energy emission peak is attributed to the $S_0 \leftrightarrow S_1$ (HOMO ↔ LUMO) transition and agrees very well (both in relative intensity and peak position) with the corresponding peak in end-capped quaterthiophene films deposited on glass (486 nm).[36] The lower energy peaks are attributed to vibronic transitions. Lack of mirror symmetry between the absorption and photoluminescence spectra suggests a different conformation for the quaterthiophene moiety in the ground and excited states. The Stokes shift, determined from the photoluminescence emission and excitation (or equally from the UV−vis absorption) spectra, is the same for each of the dye salt films and is approximately 28(3) nm (0.16 eV).

When the AEQT cation is incorporated within the layered perovskite framework, some interaction between excitations

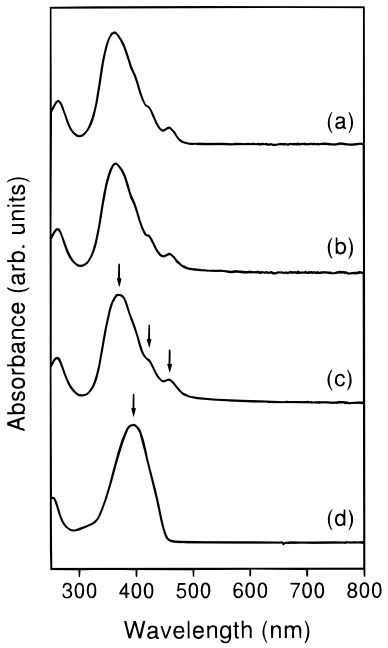

Figure 6. Room temperature UV−vis absorption spectra for thermally ablated thin films of AEQT·2HX on quartz substrates, where (a) X = Cl, (b) X = Br, and (c) X = I. The spectral features are identical and are marked with arrows for the X = I spectrum. For comparison, the absorption spectrum of AEQT·2HCl in a methanol solution (d) is also shown, with the single feature marked with an arrow.

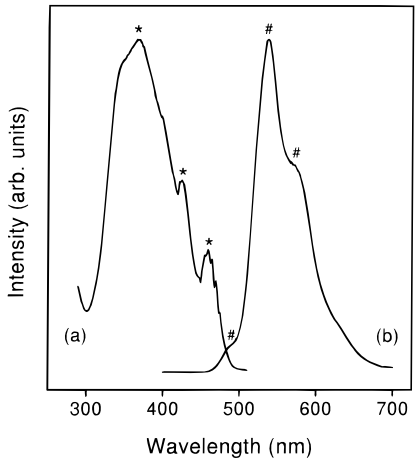

Figure 7. Room temperature photoluminescence (a) excitation (λ_{em} = 540 nm) and (b) emission (λ_{ex} = 370 nm) spectra for a thermally ablated thin film of AEQT·2HCl. The spectra for the other AEQT·2HX samples with X = Br and I are virtually identical to those of the X = Cl film. The most important features in the spectra are indicated with ∗ (excitation) and # (emission).

(33) Papavassiliou, G. C.; Koutselas, I. B. *Synth. Met.* **1995**, *71*, 1713.
(34) Gigli, G.; Rinaldi, R.; Lomascolo, M.; Cingolani, R.; Barbarella, G.; Zambianchi, M. *Appl. Phys. Lett.* **1998**, *72*, 1013.
(35) Kanemitsu, Y.; Shimizu, N.; Suzuki, K.; Shiraishi, Y.; Kuroda, M. *Phys. Rev. B* **1996**, *54*, 2198.
(36) Gebauer, W.; Väterlein, C.; Soukopp, A.; Sokolowski, M.; Hock, R.; Port, H.; Bäuerle, P.; Umbach, E., *Synth. Met.* **1997**, *87*, 127.

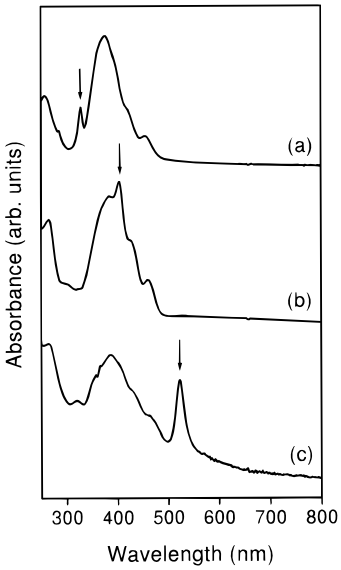

Figure 8. Room temperature UV−vis absorption spectra for thermally ablated thin films of (AEQT)PbX_4 on quartz substrates, where (a) X = Cl, (b) X = Br, and (c) X = I. The peak from the lead(II) halide sheet exciton is marked with an arrow in each spectrum.

within the dye molecule and the inorganic sheets might be expected. In fact, the absorption from the chromophore in the hybrid (Figure 8) is similar to that observed in the pure dye salt samples. The three components of the chromophore absorption band can still be made out in each of the (AEQT)-PbX_4 (X = Cl, Br, and I) films (with virtually identical spectral positions to those found in the dye salts). The exciton peak, characteristic of the inorganic sheets of corner-sharing lead(II) halide octahedra, is also observed in each absorption spectra. The peaks fall at 330(2), 404(2), and 523(2) nm for the X = Cl, Br, and I films, respectively. These values are similar to those observed for the lead(II) halide-based organic−inorganic perovskites with optically inert organic layers and demonstrate that the layered perovskite structure is formed in the ablated films. The absorption spectra also demonstrate the flexibility of the organic−inorganic perovskite framework (in this case, the ability to substitute various halides, X, into the structure) to enable tuning of the inorganic sheet exciton band position relative to the organic chromophore HOMO−LUMO transition. For X = Cl, the exciton peak is at a higher energy than the dominant chromophore absorption. For X = Br, the two energies are roughly resonant, while for X = I, the exciton absorption is at lower energy relative to the organic absorption features.

The photoluminescence emission and excitation spectra for (AEQT)PbX_4 ablated films with X = Cl are shown in Figure 9 and exhibit a strong emission peak from the quaterthiophene moiety at 532 nm. The excitation spectrum for the perovskite is almost identical with that of the dye salt with respect to both peak positions and relative intensities. Photoluminescence from quaterthiophene in the X = Br and I compounds drops precipitously in intensity across the series X = Cl to X = I. For comparison, the low temperature (T = 30 K) and ambient temperature (T = 290 K) photoluminescence emission spectra for a crystalline powder of (AEQT)$PbBr_4$ are shown in Figure 10a,b, respectively. Note the similarity between the room temperature thin film spectrum (Figure 10c) and the powder data. The additional broadening in the thin film spectrum presumably arises from the inferior crystallinity of these samples relative to the crystalline deposit. In the low-temperature powder data, the broad features present in the 290 K data substantially sharpen, enabling a more detailed investigation of the fine

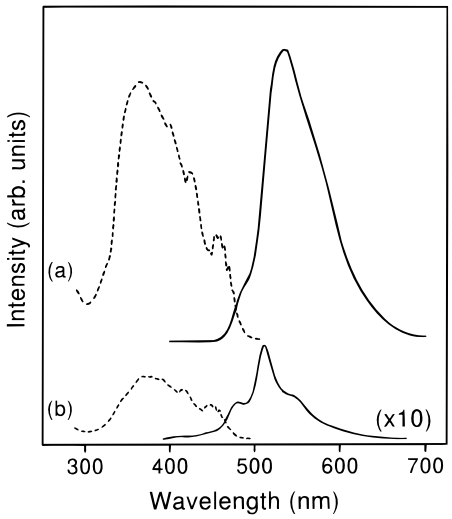

Figure 9. Room temperature photoluminescence excitation (λ_{em} = 540 nm) and emission (λ_{ex} = 370 nm) spectra for thermally ablated thin films of (AEQT)PbX_4 with (a) X = Cl and (b) X = I. Note that the intensities for the weak X = I spectra have been multiplied by a factor of 10 to enable a comparison with the X = Cl spectra.

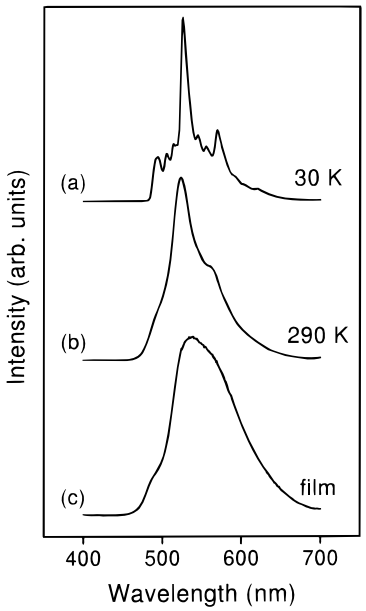

Figure 10. (a) Low-temperature (T = 30 K) and (b) near-ambient temperature (T = 290 K) photoluminescence spectra (λ_{ex} = 360 nm) for a microcrystalline deposit of (AEQT)$PbBr_4$ on a sapphire window. For comparison, (c) the room temperature photoluminescence spectrum (λ_{ex} = 370 nm) for a thermally ablated thin film of (AEQT)$PbBr_4$ is also shown.

structure of the photoluminescence spectrum. The S_0−S_1 transition at 490(2) nm (2.53 eV) is better resolved. Clearly evident as well is the vibronic fine structure of the spectrum, indicating good coupling between the electronic and vibrational modes. Especially important is the thiophene ring breathing mode, with an energy of around 1440 cm^{-1}.[36] This is evident in the low-temperature data as the dominant peak in the emission spectrum at approximately 527(2) nm, along with the second-order peak at 570(2) nm. Note that, even in the low-temperature data, there is no evidence of exciton emission from the lead(II) bromide sheets.

The relative energy gap differences between and the absolute energy positions of the chromophore HOMO−LUMO levels and the inorganic layer conduction, valence, and exciton bands

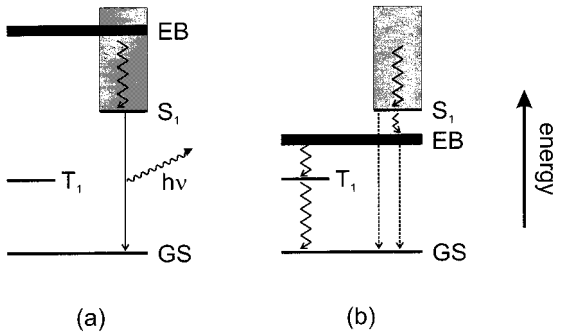

Figure 11. Schematic energy level diagrams for the $(AEQT)PbX_4$ system with (a) X = Cl and (b) X = I, as determined from the absorption data and literature values for T_1.[38] The relevant energy levels include the S_1 and T_1 states for the organic molecule (note that the gray box above the S_1 state corresponds to the vibronic progression and higher lying states for the organic molecule) and the exciton band (EB) for the inorganic framework. GS refers to the ground state for each of the transitions. The transitions in (b) that are indicated with dotted lines are either not observed (EB → GS) or only weakly observed (S_1 → GS). The zigzag lines correspond to possible nonradiative transitions. The conduction and valence bands for the lead(II) halide framework have been left off the diagram for the sake of clarity. Note that the spacing between energy levels has not been drawn to scale.

are important in understanding the fate of excitations within these perovskites. A recent study on the chromophore-containing perovskites, $(RNH_3)_2PbCl_4$ (R = phenylmethyl, 2-naphthylmethyl, and 2-anthrylmethyl), shows energy transfer between the organic and inorganic components of the hybrid.[37] The path of energy flow in these systems is described in terms of the energy differences of the singlet (S_1) and triplet (T_1) transitions of the organic chromophore and the exciton transition of the inorganic framework. Similar energetic considerations for the $(AEQT)PbX_4$ system suggest that, for X = Cl (Figure 11a), the exciton band (EB) transition (3.7 eV) of the inorganic sheets is larger than the S_1 (2.7 eV) and recently reported[38] T_1 (~1.7 eV) transitions for the quaterthiophene chromophore. Since transitions between the singlet and triplet states are optically forbidden, light emission primarily arises from the S_1-S_0 transition. For X = I (Figure 11b), the exciton transition (2.4 eV) of the lead iodide sheets is between those of the S_1 and T_1 states for the quaterthiophene moiety. If energy flow follows the same path as in the energetically similar $(C_{10}H_7CH_2NH_3)_2PbCl_4$ compound, which ends in phosphorescence from the naphthalene triplet state, emission for $(AEQT)PbI_4$ may be quenched, as the triplet state of the quaterthiophene molecule is generally nonemissive.[38]

In addition to considering only the differences between the organic HOMO−LUMO and inorganic layer exciton energy gaps (as determined from optical absorption data), knowledge of the absolute positions of these energy levels is also important. Since the organic and inorganic components form distinct layers, offsets between the energy levels of these components may lead to charge transfer. Charge transfer has been extensively studied for systems of adsorbed dyes on inorganic semiconductor surfaces.[39] In $(AEQT)PbX_4$, the X = Cl compound has the largest inorganic band gap and an emission efficiency (from

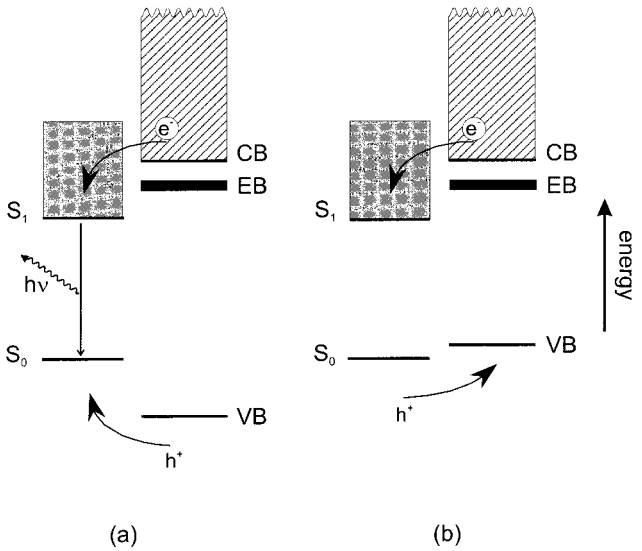

Figure 12. Schematic energy level diagrams, highlighting the fact that the organic and inorganic components of the chromophore-containing hybrids are spatially separated, as well as the possibility of different energy level alignments. The type I heterojunction (a) is drawn for $(AEQT)PbCl_4$, and the type II heterojunction (b) is a possible representation for $(AEQT)PbI_4$. The relevant energy levels include the singlet S_0 and S_1 states for the chromophore and the valence band (VB), conduction band (CB) and exciton band (EB) states for the lead (II) halide sheets. For clarity, the triplet level (T_1) has been left off of the chromophore energy level scheme. Note also that to draw this diagram, we have arbitrarily chosen an offset energy between the chromophore S_1 edge and the inorganic conduction band edge (CB).

the quaterthiophene moiety) comparable to that of the dye salt, suggesting that it may form a type I heterojunction (Figure 12a). In this case, the HOMO and LUMO levels of the quaterthiophene molecule are the lowest energy states for both electrons and holes, and the carriers may recombine radiatively in the chromophore. As X is varied to Br and I, the band gap of the inorganic component decreases and the absolute energies of the conduction, valence, and exciton bands shift relative to the HOMO−LUMO levels of the quaterthiophene molecule. Theoretical modeling of the band structure in $(RNH_3)_2PbX_4$ pervoskites (where R is optically and electrically inert) suggests that the conduction band has 98% Pb character, while the valence band has substantial halide character.[40] Varying the halogen from X = Cl to X = I therefore increases the energy of the valence band, while the energy of the conduction band remains essentially constant. This may result in a type II quantum well structure (Figure 12b) for $(AEQT)PbI_4$, where the lowest energy state for electrons and holes may be such that electrons experience a driving force toward the organic component, while holes are driven toward the inorganic component. Charge separation between the organic and inorganic components inhibits overlap of the electron and hole wave functions and may therefore decrease the probability of the carriers recombining radiatively. Studies are underway to understand the relative influence of these (and other) competing energy transfer and charge separation mechanisms on the optical properties of chromophore-containing organic−inorganic perovskites.

Conclusion

A recent thrust in the area of organic−inorganic hybrids involves the incorporation of more complex (and functional)

(37) Braun, M.; Tuffentsammer, W.; Wachtel, H.; Wolf, H. C. *Chem. Phys. Lett.* **1999**, *303*, 157.

(38) Rentsch, S.; Yang, J. P.; Paa, W.; Birckner, E.; Schiedt, J.; Weinkauf, R. *Phys. Chem. Chem. Phys.* **1999**, *1*, 1707. The T_1 value in this study was determined in the gas phase. Therefore this can only be used as a rough approximation for T_1 in the solid state.

(39) (a) Sakata, T.; Hashimoto, K.; Hiramoto, M. *J. Phys. Chem.* **1990**, *94*, 3040. (b) Miyasaka, T.; Watanabe, T.; Fujishima, A.; Honda, K. *J. Am. Chem. Soc.* **1978**, *100*, 6657.

(40) Ishihara, T.; Hirasawa, M.; Goto, T. *Jpn. J. Appl. Phys.* **1995**, *34−1 (supplement)*, 71.

molecules within an inorganic framework. In this work, we introduce one member of the family $[NH_3-R-NH_3]MX_4$, where $R = (CH_2)_nT_m(CH_2)_n$ and T_m represents an oligothiophene with "*m*" α-linked thiophenes (in this case, $n = 2$ and $m = 4$). In contrast to systems with optically inert R-groups (i.e. alkyl or single ring aromatic), which only exhibit optical properties (in the visible spectrum) associated with the metal halide layers, the current chromophore-containing hybrids display more complex optical properties. In the optical absorption spectra, the exciton features from the metal halide sheets are identified, along with characteristic absorption from the chromophore. In the photoluminescence spectrum, no evidence of the inorganic layer exciton emission is observed for the lead(II) halides. For X = Cl, strong photoluminescence from quaterthiophene can be observed. In contrast, when the inorganic layer excitonic transition is shifted to lower energy than the organic $\pi-\pi^*$ transition (i.e. for X = I), photoluminescence from the organic layer is substantially quenched. This loss of photoluminescence intensity suggests a quenching mechanism that is likely to involve energy transfer and/or charge separation between the organic and inorganic layers of the structure. Note also that since the transition dipole of the quaterthiophene moiety should be aligned along the long axis of the molecule, and given the highly ordered nature of the organic layer of the hybrid, some dichroism of the optical properties[35] should be expected in single crystals of $(AEQT)PbX_4$.

The examination of the oligothiophene-containing hybrid family with different *n* and *m* is an area of future interest. Increasing *n* is expected to decrease the coupling between the organic and inorganic structural components, while modifying *m* can be used to vary the HOMO−LUMO gap of the chromophore. Finally, by selecting different metal halide frameworks (MX_4^{2-}), the band gap of the inorganic layers can be tuned over a wide range relative to the HOMO−LUMO gap of the chromophore. In addition to the fundamental interest of such systems in terms of addressing energy/charge transfer in organic−inorganic hybrids, the oligomer-containing hybrids also offer opportunities in the area of electronic devices. Recently, a light emitting diode (LED) based on the $(AEQT)PbCl_4$ organic−inorganic perovskite has been demonstrated[41] and relatively efficient electroluminescence has been observed at room temperature. The room temperature operation of these devices is in contrast to LEDs based on organic−inorganic perovskites containing optically inert organic molecules, which only operate at low temperature.[42]

Other opportunities can be envisioned in the study of electrical transport in ordered oligothiophene layers and organic−inorganic FETs (devices with an organic−inorganic hybrid as the channel material),[43] where in this latter case the electrical transport can either be in the oligomer layer or the inorganic layer. In the current system, the quaterthiophene molecules are found to pack as a single crystalline layer between the lead(II) halide sheets. The packing of the quaterthiophene moieties within a layer is in a herringbone fashion, similar to many other crystalline aromatic organic systems. However, the quaterthiophenes adopt a somewhat unusual, nearly planar syn−anti−syn conformation between adjacent thiophene rings, presumably as a result of the hydrogen bonding and aromatic interactions holding the molecule in the framework. Future work will focus on how the inorganic framework can be used to template the organic cations and therefore control the optical and electrical properties of the organic layers. In addition, the effect of varying *n* or *m* on the conformation and orientation of the oligomer within the current family of materials will also be of interest.

Acknowledgment. The authors gratefully acknowledge DARPA for partial support of this work under Contract DAAL01-96-C-0095.

Supporting Information Available: Tables providing a full listing of experimental and crystallographic data (Table S.1), all atomic coordinates (Table S.2), and anisotropic temperature factors for all non-hydrogen atoms (Table S.3). This material is available free of charge via the Internet at http://pubs.acs.org.

IC991048K

(41) Chondroudis, K.; Mitzi, D. B. *Chem. Mater.* **1999**, *11*, 3028.

(42) Era, M.; Morimoto, S.; Tsutsui, T.; Saito, S. *Appl. Phys. Lett.* **1994**, *65*, 676.

(43) Kagan, C. R.; Mitzi, D. B.; Dimitrakopoulos, C. D. *Science* **1999**, *286*, 945.